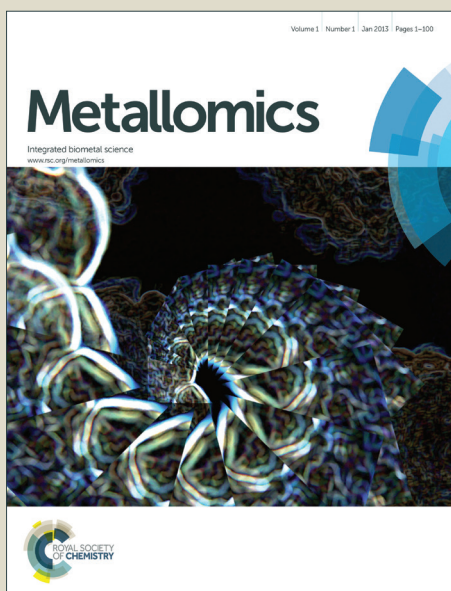


Metallomics

Accepted Manuscript



This is an *Accepted Manuscript*, which has been through the Royal Society of Chemistry peer review process and has been accepted for publication.

Accepted Manuscripts are published online shortly after acceptance, before technical editing, formatting and proof reading. Using this free service, authors can make their results available to the community, in citable form, before we publish the edited article. We will replace this *Accepted Manuscript* with the edited and formatted *Advance Article* as soon as it is available.

You can find more information about *Accepted Manuscripts* in the [Information for Authors](#).

Please note that technical editing may introduce minor changes to the text and/or graphics, which may alter content. The journal's standard [Terms & Conditions](#) and the [Ethical guidelines](#) still apply. In no event shall the Royal Society of Chemistry be held responsible for any errors or omissions in this *Accepted Manuscript* or any consequences arising from the use of any information it contains.

1
2
3
4 **Understanding metal homeostasis in primary**
5 **cultured neurons. Studies using single neuron**
6 **subcellular and quantitative metallomics.**
7
8
9

10
11
12 **Robert A. Colvin¹, Barry Lai², William R. Holmes¹, Daewoo Lee¹**
13

14
15 ¹Department of Biological Sciences, Ohio University, Athens, OH 45701, USA
16

17 ²X-Ray Science Division, Argonne National Laboratory, Argonne, IL 60439, USA
18
19
20
21
22
23
24
25
26
27
28
29
30
31
32
33
34
35
36
37
38
39
40
41
42
43
44
45
46
47
48
49
50
51
52
53
54
55
56
57
58
59
60

Abstract:

The purpose of this study was to demonstrate how single cell quantitative and subcellular metallomics inform us about both the spatial distribution and cellular mechanisms of metal buffering and homeostasis in primary cultured neurons from embryonic rat brain, which are often used as models of human disease involving metal dyshomeostasis. The present studies utilized synchrotron radiation X-ray fluorescence (SRXRF) and focused primarily on zinc and iron, two abundant metals in neurons that have been implicated in the pathogenesis of neurodegenerative diseases such as Alzheimer's disease and Parkinson's disease. Total single cell contents for calcium, iron, zinc, copper, manganese, and nickel were determined. Resting steady state zinc showed a diffuse distribution in both soma and processes, best defined by the mass profile of the neuron with an enrichment in the nucleus compared with the cytoplasm. Zinc buffering and homeostasis was studied using two modes of cellular zinc loading – transporter and ionophore (pyrithione) mediated. Single neuron zinc contents were shown to statistically significantly increase by either loading method – ionophore: 160 million to 7 billion; transporter 160 million to 280 million atoms per neuronal soma. The newly acquired and buffered zinc still showed a diffuse distribution. Soma and processes have about equal abilities to take up zinc via transporter mediated pathways. Copper levels are distributed diffusely as well, but are relatively higher in the processes relative to zinc levels. Prior studies have observed iron puncta in certain cell types, but others have not. In the present study, iron puncta were characterized in several primary neuronal types. The results show that iron puncta could be found in all neuronal types studied and can account for up to 50% of the total steady state content of iron in neuronal soma. Although other metals can be present in iron puncta, they are predominantly iron containing and do not appear to be associated with ferritin cages or transferrin receptor endosomes. The iron content and its distribution in puncta were similar in all neuron types studied including primary dopaminergic neurons. In summary, quantitative measurements of steady state metal levels in single primary cultured neurons made possible by SRXRF analyses provide unique information on the relative levels of each metal in neuronal soma and processes, subcellular location of zinc loads, and have confirmed and extended the characterization of heretofore poorly understood cytoplasmic iron puncta.

Introduction:

Quantitative metallomics of single cultured cells has recently been made possible with the development of high-energy synchrotron X-ray beams like that available at the Advanced Photon Source facility (APS, Argonne National Laboratory, Argonne, IL). The submicron resolution and sensitivity of synchrotron radiation X-ray fluorescence (SRXRF) technique provides the means to scan single cells and generate high resolution 2-D maps of their metal distributions. In addition, SRXRF is quantitative, allowing the unique opportunity to quantify and localize metals *in situ* in individual cultured cells.^{1,2} This powerful technique has now been used to map and quantify metals in their cellular microenvironment using many different tissues and cell types including cultured rodent primary neurons³⁻⁵. Metal dyshomeostasis is known to accompany human neurological disorders such as Alzheimer's disease and Parkinson's disease, however not enough is known about normal metal homeostasis in neurons, thus limiting our understanding of the significance of the observed alterations in metal levels on disease pathogenesis.⁶⁻¹⁰

1
2
3 Cultured rodent primary neurons and SRXRF analyses provide experimenters with a unique window to
4 study single cell metal homeostasis under both normal conditions and as models of human
5 neurodegenerative diseases such as Alzheimer's disease, and Parkinson's disease. A better
6 understanding of the subcellular distribution and metal composition of primary neurons will expand the
7 utility of these models to study cellular mechanisms of metal dyshomeostasis implicated in these
8 diseases.
9

10
11 Understanding of the intracellular distribution and levels of "free" cytosolic and organellar zinc in
12 primary neurons has advanced considerably due to the availability of cell permeable and genetically
13 targeted fluorescent sensors¹¹⁻¹³ however, these methods can not quantify the total cellular zinc
14 content, map the entire cell, or provide "metallomic" data on the levels of zinc and other metals as a
15 result of changing intracellular zinc levels. As mentioned above, only a few studies have been published
16 using SRXRF to analyze the subcellular distribution and zinc content of primary cultured neurons. This
17 study provides a significant advance from previous studies, as a complete analysis of the metallo-
18 me of primary cultured neurons is described both before and after neurons are challenged with zinc loads.
19

20
21 Iron in primary cells has been studied more extensively by SRXRF especially in relation to its potential
22 role in the death of dopaminergic cells in Parkinson's disease.^{9,10} Iron puncta are observed after iron
23 exposure in PC12 cells (with or without nerve growth factor treatment) in both a peri-nuclear location
24 and in cellular processes^{14,15}. Another study using primary dopaminergic neurons⁴ found a low and
25 uniform subcellular distribution of iron in the soma. Although this study focused on iron speciation, no
26 evidence for iron puncta was presented. Finally, a recent study utilizing primary cortical cultured
27 neurons from mice³ reported iron puncta in the soma of these neurons. The present study extends
28 these studies providing additional evidence for the presence of iron puncta and provides a much more
29 detailed quantitative analysis of iron levels in neuronal soma and puncta in several primary cultured
30 neuronal types including dopaminergic neurons.
31
32

33 **Methods:**

34
35 **Primary neuron cultures:** All procedures involving animals were approved by the Ohio University IACUC.
36 Primary cultures of neurons were grown on silicon nitride windows (SiN, Silson, Ltd. UK) that were
37 pretreated with a polyethyleneimine solution to improve cell adherence. *Embryonic rat cortical or*
38 *hippocampal cultures:* The methods for culture of well characterized embryonic rat primary cortical or
39 hippocampal cultures are described in detail in published works^{16,17}. Briefly, brains are removed from
40 the skulls and kept moist in Hank's balanced saline solution (without Mg²⁺ and Ca²⁺) (HBSS) for further
41 dissection. Using a dissecting microscope, the cerebral cortex was carefully separated, using blunt
42 dissection, from the brainstem, diencephalon, olfactory bulbs, and cerebellum, which were discarded.
43 Next the meninges and choroid plexus were stripped away. The cerebral hemispheres and hippocampi
44 were separated and cut into small pieces and trypsinized in HBSS at room temperature. After
45 trypsinization, nerve cells were dissociated by gentle trituration through the arrow opening of a fire
46 polished Pasteur pipette. The dissociated neurons suspended in HBSS were added to 24 well culture
47 plates (Falcon) containing SiN windows coated with polyethylenimine (50% solution, Sigma, St. Louis,
48 MO, USA), which was diluted 1:1000 in borate buffer. The cortical neurons are allowed to attach to the
49
50
51
52
53
54
55
56
57
58
59
60

1
2
3 surface at 37°C, 5% CO₂ in 0.5 ml of MEM solution (Cellgro) supplemented with 10mM sodium
4 bicarbonate, 2 mM L-glutamate, 1 mM pyruvate, 20 mM KCl and 10% (v/v) heat inactivated fetal bovine
5 serum. After 3 to 6 h, the media was switched to neurobasal media (Life Technologies) supplemented
6 with 0.5 mM glutamine and 2% B-27 (Gibco BRL). *Embryonic rat ventral midbrain cultures*: Primary
7 cultures containing a mixture of dopaminergic and non-dopaminergic ventral midbrain neurons were
8 prepared from E13-14 fetal brains as described previously¹⁸. The procedure described above was
9 followed except dissociated neurons were plated on SiN windows directly into Neurobasal media
10 supplemented with 2% B-27. Both types of cultures were maintained at 37°C in 5% CO₂, maintained in
11 Neurobasal media supplemented with 2% B-27.
12
13
14
15

16
17 **Sample preparation for synchrotron radiation x-ray fluorescence analysis (SRXRF analysis):** After 4-6
18 days in vitro (DIV) when cell growth had mostly stabilized, experimental manipulations were performed.
19 Just prior to experimental manipulations, the neurons were incubated with 125 nM MitoTracker® Green
20 (Life Technologies) for 45 min at 37°C. The MitoTracker® Green labels mitochondria and allowed better
21 visualization of cell morphology and evaluation of the integrity of subcellular structure in individual
22 neurons that were eventually selected for SRXRF analysis. After experimental manipulations were
23 completed, neurons were washed three times in ice-cold wash buffer (154 mM NaCl, 5.6 mM KCl, and
24 26 mM NaHCO₃, 100 µM EDTA, chelex treated, pH 7.4). After this wash was complete, neurons attached
25 to SiN were fixed by one of two methods: chemical fixation – 8 min in aqueous 4% formaldehyde
26 dissolved in phosphate buffered saline (PBS) and chelex treated, or cryofixation – either manual plunge
27 freezing in 2-methylbutane cooled in liquid N₂ or block freezing by placing the SiN on dry-ice powder.
28 Chemically fixed neurons were washed three times in PBS (chelex treated) then were dehydrated by one
29 of two methods: either air-drying in a desiccated chamber¹⁹ or a series of 1 min washes in increasing
30 acetone (30%, 50%, 70%, 95%, 100%, 100%). Cryofixed neurons were dehydrated by lyophilization for
31 several hours. All samples were subsequently stored at room temperature under vacuum in a desiccator
32 and used within one week for SRXRF analysis. The method of fixation used is noted in each figure
33 legend.
34
35
36
37
38
39

40 **SRXRF analysis of single neurons:** The equipment required for SRXRF analysis is available as part of the
41 general user facility at the Advanced Photon Source (APS, Argonne National Laboratory, Argonne, IL)
42 beamline 2-ID-D. To locate neurons on SiN windows for later SRXRF analysis, the neurons were
43 visualized first by epifluorescence using an optical microscope (Leica DMXRE). Neurons chosen for later
44 SRXRF analysis were those judged to have intact subcellular structure by having a normal distribution of
45 MitoTracker® Green fluorescence within the peri-nuclear region of the soma and within individual
46 processes. The x/y coordinates of the neurons selected could be referenced to the same points on the
47 SiN window once mounted in the 2-ID-D beamline. A monochromatic X-ray beam was focused on the
48 specimen using a Fresnel zone plate. Excitation energy was 10 keV allowing excitation of zinc,
49 potassium, sulfur, and other transition elements. A scan area was selected based on the boundaries of
50 the cell determined both by a coarse 2-D scan viewed using the MAPS software (see below) and the
51 MitoTracker® Green epifluorescence image of the same cell. A final high resolution scan was performed
52 at 25°C under He atmosphere with a pixel step size of 0.3 µm and a 1 sec dwell time. A high resolution
53 scan of an average sized cultured neuron generally required several hours to complete.
54
55
56
57
58
59
60

1
2
3
4
5 **SRXRF data analysis:** Because the X-ray fluorescence energy is specific for each element, the spectrum
6 provides unambiguous information about elemental contents of the scanned neuron. Spectral fitting
7 and background correction of the elemental fluorescence peaks were performed as described
8 previously²⁰. Elemental fluorescence peak signals were calibrated with a NIST (National Institute of
9 Standards and Technology, Gaithersburg, MD) standard prior to a scan session. Analysis of the raw data
10 2-D image is performed with the MAPS software²¹. All SRXRF data presented in this study is background
11 subtracted. The high resolution 2-D scan and matching epifluorescence image were used to identify a
12 region without cellular material. This region was carefully outlined manually as a region of interest (ROI)
13 and the mean metal content calculated (ng/cm²) for each metal analyzed. This value was subtracted
14 from the mean metal content obtained from ROIs drawn around the soma or processes in the same scan
15 area. This is the best blank that can be utilized since it gets all the same experimental treatments. The
16 MAPS software has a drawing tool that allows an ROI to be manually drawn around any region in the
17 scan and quantified. The MAPS software allows line scan data to be obtained from 2-D scans. Using the
18 software, a line is manually drawn anywhere in the 2-D image and fluorescence intensities for each
19 element along the trajectory of that line are reported.
20
21
22
23
24
25

26 **Zinc loading:** Cultured neurons were washed free of Neurobasal/B-27 supplemented media and
27 incubated at 37°C in a physiological buffer to which 30 μM ZnCl₂ (3 minutes) or 30 μM ZnCl₂/5 μM
28 pyrithione (30 minutes) were added. The treatment conditions are described in greater detail in
29 a previous publication¹¹.
30
31
32

33 **Immunofluorescence and MitoTracker® Green fluorescence:** The methods used for
34 immunofluorescence, epifluorescence visualization, and image capture of primary neurons on glass
35 coverslips or SiN windows are published elsewhere^{16,22}. Antibodies for transferrin receptor (CD71) and
36 ferritin light chain were obtained from Santa Cruz Biotechnology; and for LC3B from Cell Signaling
37 Technology.
38
39
40

41 **Statistical analysis:** In figures where mean metal contents of ROIs are compared, these data were
42 derived from manually drawn ROIs (see methods above) averaged using scans obtained from separate
43 visits to the 2-ID-D beamline at APS. The number of single neurons used to calculate the mean is
44 indicated in parentheses in the figure and/or listed in the figure legend as well. When appropriate,
45 student's t test or one-way ANOVA with Tukey's posttest were used to derive *p* values to test the
46 significance of the observed differences in the calculated means. *p* values are listed in the figure
47 legends.
48
49
50

51 **Results:**

52
53
54 **Subcellular distribution of metals – neuronal soma.** As outlined in the introduction, SRXRF analysis is a
55 powerful technique allowing the simultaneous analysis of steady state metal levels in single neurons and
56 the elucidation of the subcellular distribution of each of those metals. Subcellular metal distributions
57
58
59
60

1
2
3 were obtained in this study for both the soma of single neurons and the neuronal process network that
4 surrounds individual neurons in culture. It is well documented that choice of sample preparation
5 method influences to a variable degree the retention of each metal analyzed; both increased and
6 decreased metal levels have been observed.^{5,23-26} Supplementary figs. S1-3 quantify the effect of sample
7 preparation method on metal retention as determined in SRXRF scans of single cortical neurons grown
8 on SiN windows in this study.
9
10

11
12 A 2-D scan for zinc of a representative resting neuronal soma is shown in fig. 1A. In this figure metal
13 levels (ng/cm^2) are shown using a rainbow scale. Zinc had a diffuse distribution in the cytoplasm and
14 nucleus and tracked well with cellular mass. Iron was strikingly different in its subcellular distribution
15 (fig. 1E). Iron, while having a measureable uniform concentration in the cytoplasm and nucleus, was
16 found also in several (per neuron) puncta that were observed in a peri-nuclear location. Note the puncta
17 visible in the upper right corner of fig. 1E, which includes puncta visible in a neighboring neuron. Nearly
18 every neuron scanned demonstrated at least one puncta highly enriched for iron. Iron puncta have a
19 size of 1.62 ± 0.14 (chemical fixation) and 1.72 ± 0.17 (cryofixation) μm^2 (mean \pm S.E.).
20
21
22
23

24
25 A second way of illustrating the subcellular distribution of metals is to use the line scan function in the
26 MAPS software. Figs. 1H-L plot metal concentration (ng/cm^2) along a line manually drawn across the
27 center of the cell and directly over iron puncta (see 2-D scan with red arrow). Further confirmation that
28 zinc is diffusely distributed in the neuronal soma is shown in figs. 1H&D. Here the line scans for sulfur
29 and phosphorous are overlaid with zinc. Sulfur is generally accepted to be uniformly distributed in the
30 cytoplasm and mostly track cellular mass. Zinc can be seen to follow the mass profile of the cell, but can
31 be seen to be enriched in the nucleus when compared with sulfur (see arrows in fig. 1H). The
32 phosphorous profile matches the zinc profile and would be enriched in the nucleus as well. In contrast,
33 when zinc is overlaid with either iron or calcium clear differences in the cellular distributions are
34 evident, particularly for iron (compare figs. 1J with H), which clearly show puncta highly enriched for
35 iron in a peri-nuclear location. Finally, fig. 1L shows an overlay of iron and calcium that clearly shows the
36 unique cellular distribution of each metal. Quantitative metallomics demonstrates that the subcellular
37 iron puncta are highly enriched in iron and no other metal shows the same degree of enrichment (see
38 figs. 2A&B). Whereas zinc shows a small exclusion from iron puncta, the other metals studied (except for
39 calcium) show variable and small degrees of enrichment in the iron puncta. Regardless, the SRXRF data
40 support the contention that iron puncta are intracellular structures highly enriched and selective for
41 iron.
42
43
44
45
46
47

48
49 We next searched for experimental evidence that could relate these iron enriched puncta to known
50 cellular structures associated with iron homeostasis. Iron-sulfur clusters are a primary source of iron-
51 sulfur for protein biosynthesis and iron for redox function in cells and are created by a complex
52 biosynthetic pathway.^{27,28} Perhaps, the puncta we observed could be aggregates of iron-sulfur clusters.
53 Iron-sulfur clusters are composed of 2Fe-2S units, so generally should have equimolar amounts of iron
54 and sulfur. SRXRF analysis of iron puncta show clear enrichment of iron, but sulfur is at the same level as
55 the rest of the cell body or slightly elevated only. The slight elevation of sulfur could represent additional
56 protein associated with these structures, but argues against the predominant iron species to be iron-
57
58
59
60

1
2
3 sulfur clusters. Only traces of sulfur are found enriched in puncta. Cytosolic ferritin cages are thought to
4 be the primary storage site of cellular iron. They are thought to store up to 4,500 iron atoms per cage.⁹
5 Once again, the iron puncta we observed could be aggregates of ferritin cages. To test this hypothesis
6 we used ferritin specific antibodies and immunofluorescence to localize ferritin in cultured neurons (fig.
7 3A). Ferritin had a uniform particulate distribution in the cytosol of the neuronal soma, consistent with
8 its primary role as a means of cytosolic storage of iron. Evidence of larger aggregates (approximately 1
9 micron in diameter) of ferritin in a peri-nuclear location were occasionally observed (see arrows fig. 3A),
10 but were not seen with the same regularity as seen for iron puncta in SRXRF scans. Thus, ferritin
11 immunofluorescence is inconsistent with the notion that the iron puncta seen in SRXRF are the result of
12 ferritin aggregates. Published reports note that ferritin cages are recycled by a process of autophagy via
13 fusion with autophagosomes²⁹ and can be identified by co-localization of ferritin with LC3B antibodies.³⁰
14 We tested this hypothesis by double labeling resting neurons with both ferritin and LC3B antibodies.
15 However, immunofluorescence of resting neurons failed to show significant co-localization between
16 these two antibodies (figs. 3B-D) in a peri-nuclear location. Iron enters neurons as it does in most cells
17 via transferrin receptor endocytosis.⁹ Transferrin receptor endosomes could contain significant amounts
18 of iron before export by DMT1. To test this hypothesis, the location of transferrin receptor antibodies in
19 cultured neurons was determined by immunofluorescence (figs. 3E-G). Transferrin receptor antibodies
20 were localized to neuronal processes and in the soma plasma membrane and interestingly in the nuclear
21 membrane. These data make it unlikely that transferrin receptor endosomes are responsible for the iron
22 containing puncta observed by SRXRF.
23
24
25
26
27
28
29
30

31 **Subcellular distribution of metals – neuronal processes:** The excellent subcellular resolution of SRXRF
32 allows an analysis of the metal contents of neuronal processes providing an opportunity to contrast
33 metal distributions found in processes with that found in the soma. Processes were well defined using
34 the zinc scans, thus the zinc scans were used to outline neuronal processes and the same ROIs
35 transferred to the other metal scans. When analyzing SRXRF scans with well defined neuronal processes,
36 it was found that the relative levels of the most abundant metals was nearly identical to that seen in the
37 soma (see fig. 4). Unfortunately, the lower cellular mass of processes and the lower metal content of
38 trace metals prevented accurate analysis of the less abundant metals in processes. The most abundant
39 metals were best characterized as uniformly distributed in processes, including iron. The assumption
40 would be that the average concentration of abundant metals in processes was similar to that found in
41 the neuronal soma. However, when comparing the ratio of zinc to copper in processes with that
42 determined for the soma, it was found that copper, relative to zinc levels, was much higher in the
43 processes (Table I – see³¹) This suggests an enrichment of copper in the processes relative to the soma
44 and could indicate relatively higher levels of copper being associated with synaptic regions.
45
46
47
48
49
50

51 **The effect of zinc loading on metal levels and distributions in cortical neurons:** Neurons were loaded
52 with zinc by two methods to determine the change in steady state zinc concentration and distribution
53 within single neurons. Both methods replaced culture media with a physiological buffered saline and
54 used micromolar concentrations of zinc added (see methods).¹¹ The first method, used treatment with
55 zinc and the ionophore pyrithione, in this case zinc uptake is rapid and neurons were exposed to these
56 conditions for 30 min at 37°C to achieve maximal loading and near full occupation of all intracellular zinc
57
58
59
60

1
2
3 binding sites in a neuron. This procedure allows the estimation of the total capacity for zinc binding in a
4 neuron. It should be remembered that both zinc and pyrithione enter the cell, but the total uptake of
5 zinc that is observed shows that zinc is off-loaded from pyrithione and is found in high levels throughout
6 the soma presumably bound to cellular ligands.¹¹
7
8

9
10 Exposure to zinc and pyrithione resulted in a large and significant increase in zinc content, average
11 steady state zinc content increased from approximately 160 million to 7 billion atoms (or 7 mM average
12 concentration) at the end of the 30 minute exposure period (fig. 5A). It should be noted that 5 μ M
13 pyrithione equates to approximately 5 million atoms inside the neuron and thus 2.5 million total zinc
14 atoms are needed to saturate all pyrithione zinc binding sites. After 30 minutes, the neurons still
15 appeared morphologically intact and were indistinguishable from untreated neurons except for the
16 increased intracellular zinc. The zinc is diffusely distributed in a resting neuronal soma (see fig. 1) and
17 this is still true even in the extreme case of maximal zinc loading with zinc and pyrithione. With zinc and
18 pyrithione treatment the zinc profile is noticeably flattened, reflecting a uniform placement of high
19 levels of zinc throughout the cytoplasm and the nucleus of the zinc and pyrithione treated neuron (ZP30
20 – see fig. 5C). Figs. 5A&B show the effect of zinc loading with pyrithione on the levels of zinc and other
21 metals in the soma. Interestingly, all metals except iron showed small significant increases and copper
22 levels experienced a large increase, from 8 million to 100 million atoms. Pyrithione binds copper with
23 high affinity, thus adventitious metal contamination in the high quality reagents and water used in these
24 studies combined with the high sensitivity of SRXRF analysis permitted detection of the uptake of these
25 metals when zinc and pyrithione were added. Thus, it important for researchers to be aware of the
26 potential uptake of significant amounts of “other” metal ions when exposing cells to zinc and pyrithione,
27 even when care is taken to avoid metal contamination. Lastly, zinc atoms loaded with pyrithione do not
28 appear to accumulate in the iron puncta, although zinc content in iron puncta was slightly elevated after
29 zinc and pyrithione, the difference was not significant ($p = 0.17$; see fig. 6).
30
31
32
33
34
35
36

37
38 In contrast, when neurons were loaded with zinc using transporter mediated uptake – a method that
39 results in a modest and relatively slower uptake of zinc, the results were noticeably different (figs. 5 &
40 7). A brief 3 minute exposure to 30 μ M zinc (a treatment that results in measureable changes in
41 cytosolic “free” zinc concentration as assessed using cell permeable zinc selective fluorophores¹¹)
42 resulted in a significant increase in total zinc atoms from about 160 million to about 280 million. No
43 other metal showed a significant change under these conditions. In the same time span, fluorescent
44 imaging studies estimate that the cytosolic “free” Zn concentration is changing but a few nanomolar, a
45 total change of a few thousand zinc atoms only! Thus, under these conditions, the neuron is able to
46 rapidly buffer nearly all the zinc load – only 0.001% of the zinc load remains “free.” The appearance and
47 distribution of zinc inside neurons after transporter mediated zinc loading provides unique insight into
48 what is happening to the newly acquired zinc. It can be seen that newly acquired zinc remains mostly
49 uniformly distributed throughout the soma. It would appear from SRXRF line scan analysis that a greater
50 proportion of the newly acquired zinc remains in the cytoplasm (note arrows in fig. 7C), suggesting that
51 the rapidly acting zinc buffer(s) are mostly located in the cytoplasm.
52
53
54
55
56
57
58
59
60

Contrasting transporter mediated zinc uptake in neuronal processes with that in the soma.

Transporter mediated zinc uptake measured in processes was similar to that observed in the soma (see fig. 8). This figure shows that the “amount” of zinc increase was similar (ng/cm^2) when comparing randomly selected regions of processes, which could be confidently outlined using the MAPS software, to somas in the same scans. The amount of transporter mediated zinc uptake is dependent on the number of functional transporters. Since zinc content and thus uptake is normalized to surface area (ng/cm^2), it would be expected that if transporter surface density was similar in processes and somas, then the amounts of zinc uptake normalized to membrane surface area would be similar as well, as was observed in 2-D SRXRF scans.

Analysis of iron levels and distribution in primary cultured dopaminergic neurons. The method used for primary culture of dopaminergic neurons yields a mixture of dopaminergic and non-dopaminergic neurons. To positively identify dopaminergic neurons, tyrosine hydroxylase immunofluorescence was used – a representative image is shown in fig. 9A. Positive staining for tyrosine hydroxylase is observed in dopaminergic neurons only. The nucleus of non-dopaminergic midbrain neurons in the same culture are visible with DAPI fluorescence. Both dopaminergic and non-dopaminergic neurons on the same SiN window were scanned by SRXRF. Because dopaminergic neurons needed to be identified by immunofluorescence, we could use chemical fixation only as a sample preparation method. In addition, we used acetone washes for dehydration (see methods). We found that chemically fixed, individual, cultured dopaminergic, non-dopaminergic midbrain, and hippocampal neurons showed no significant differences when comparing mean metal contents for zinc, copper manganese, or nickel (see figs. 9B&C) and had similar relative metal levels as cortical neurons. Since intracellular iron levels are thought to play a role in neurodegeneration of dopaminergic cells in Parkinson’s disease,^{9,10} we compared the subcellular distribution of iron and its total level in dopaminergic, non-dopaminergic midbrain, and hippocampal neurons. All neurons exhibited peri-nuclear iron puncta, enriched in iron, similar to that seen in cortical cultures. Although there was a trend toward higher levels of iron in puncta and the average concentration in the soma for dopaminergic and non-dopaminergic mid-brain neurons when contrasted with hippocampal cells, there was no significant difference in the means when analyzed by one-way ANOVA with Tukey’s posttest (fig. 9D).

Discussion:

Insights from total zinc determinations in single neurons: Estimates of total metal content (expressed as total atoms) of single cortical neurons was derived from an analysis of the soma only. Only a small correction should need be applied to account for the processes. These data allow one to make reasonable estimates of the average concentration of zinc in the soma of a cultured nerve cell. The current estimates are consistent with estimates derived from ICP-MS analysis of cortical cultures, calculated and reported previously.¹¹ It is often reported that the average volume of a cultured neuron soma is about $1,000$ to $2,000 \mu\text{m}^3$ (somewhat smaller than cells in intact tissues). The average total zinc content of neuronal somas determined in the present study is between 100 and 200 million atoms. This would equate to an average zinc concentration of about 100 to $200 \mu\text{M}$ for a neuronal soma with volume of $1,000 \mu\text{m}^3$, consistent with previously published reports.^{11,32} At the generally accepted

1
2
3 cytosolic “free” zinc concentration of about 100 pM, then just 100 “free” zinc atoms exist in the
4 neuronal soma – just .0001% of the total zinc in the soma is “free” cytosolic zinc. Interestingly,
5 considering that sample preparation differences lead to as much as 50% variation in zinc content (see
6 supplementary data), it is reasonable to suggest that 50% of the bound zinc is “diffusible” or “labile.”
7 This “diffusible” or “labile” zinc pool could be of critical importance to the generation of zinc signals and
8 maintenance of physiological zinc-protein interactions. In our published model of neuronal zinc
9 homeostasis,¹¹ a cytosolic “muffler” pool of bound zinc was utilized and could be associated with the
10 cytosolic “diffusible” zinc pool identified by SRXRF (see below for additional discussion of the model).
11
12
13
14

15 The 2-D scans derived from SRXRF analysis yield very precise determinations of the dehydrated neuronal
16 soma size. This value varied only slightly for the individual neurons scanned and was not significantly
17 different when comparing cryofixed to chemically fixed cells. The mean value of all resting and
18 untreated neurons (regardless of fixation method) was 134 μm^2 . Thus, for a hydrated volume of 1,000
19 μm^3 the hydrated neuronal soma should have an average thickness of 7.5 μm (assuming nominal
20 shrinkage in the breadth dimensions of the soma). The actual thickness of the dehydrated neuron is
21 necessarily less. It has been reported that dehydrated PC12 cells have an average thickness of 3 μm ³³
22 and an average zinc concentration of 50 ng/cm^2 .
23
24
25
26

27 It is informative to compare the total metal contents (i.e., atoms per neuron), for each of the metals
28 studied here with zinc and consider total metal contents as a physiologically regulated quota that may
29 be generalizable to most other metazoan cells. Table II lists total average metal quotas determined for a
30 single cortical neuron for each of the metals studied here. Since the vast majority of intracellular zinc is
31 “protein-bound” it is clear that a cell’s zinc quota is intricately dependent on its proteome. The metal
32 quotas of individual cells therefore depend on the fidelity and specificity of protein-metal binding sites³⁵
33 What is not so clear – is why the zinc quota of an individual metazoan cell should be 100 - 200 million
34 atoms and what prevents random interactions between metals and metal binding proteins that would
35 disrupt this finely tuned balance?³⁵ Steady state and long term changes in cytosolic “free” zinc or the
36 zinc quota would result from changes in protein expression. On the other hand, transient and short term
37 changes in cytosolic “free” zinc are likely produced by modifying the binding affinity of existing zinc
38 binding proteins or by an influx of new zinc to the cytosol from an intracellular or extracellular source.
39 Similar concepts apply to intra-organellar zinc levels as well.
40
41
42
43
44
45

46 **Insights from iron determinations in single neurons:** All types of neurons studied here, regardless of
47 sample preparation method showed a unique subcellular distribution for iron highly enriched in several
48 peri-nuclear puncta. SRXRF fluorescence allowed us to easily estimate the iron content and size of these
49 subcellular structures. The average total iron quota for a neuron as measured by SRXRF is 120 million
50 atoms (see table II) and the average number of iron atoms per puncta is 20 million (taking into
51 consideration a subtraction for average soma iron content). Since most neurons contain several puncta,
52 the puncta may account for at least half of all iron atoms that exist in the soma.
53
54
55

56 Are iron puncta an artifact of sample preparation? Several lines of reasoning argue against the
57 appearance of iron puncta being the direct result of sample preparation. First, three methods of
58
59
60

1
2
3 dehydration were used: air drying, lyophilization, and acetone washes, and two types of fixation used:
4 chemical fixation and cryofixation – each method resulted in nearly identical results. Second, there is not
5 a satisfying chemical explanation for how such an artifact could arise predominantly in the soma and
6 only for iron, i.e., iron puncta were never found in the nucleus. Third, it might be expected that such an
7 artifact would be seen for other metals as well, especially zinc, since zinc has equal or greater
8 abundance inside the cell and binds avidly to structures that can bind iron. In fact, the Irving-Williams
9 series³⁶ predicts that such coordination environments should *prefer* zinc over iron. Thus, these
10 intracellular structures seem unlikely to be an artifact of sample preparation.
11
12
13
14

15 We noted the occasional appearance of aggregates of ferritin cages in cultured neurons (see fig. 3A),
16 with a size similar to that of iron puncta. However for aggregates of ferritin cages to reach the level of 20
17 million iron atoms would require 1,000s of ferritin cages to aggregate (since ferritin cages are thought to
18 contain 4,000 – 5,000 iron atoms each). This was not the visual impression from immunofluorescence –
19 rather a handful at most.
20
21
22

23 Siderosomes are previously characterized organelles that are most often observed upon ultrastructural
24 analysis of tissues subjected to iron overload, as a result of experimental manipulations or disease.³⁷ The
25 siderosome is a single membrane organelle, with a peri-nuclear cytoplasmic location containing high
26 levels of iron, which can be detected as electron dense material in transmission electron microscopy and
27 by the Prussian-blue staining. The iron content of siderosomes is confirmed by x-ray probe analysis;
28 iron being the one and only prominent metal present and have a size about 1 micron in diameter³⁸. The
29 iron is thought to be present as ferric hydroxide. The puncta observed in SRXRF scans do fit the
30 ultrastructural description of siderosomes. Much less is understood about the origins of siderosomes,
31 but they appear to be of a lysosomal origin and are not ferritin cages. The pathobiology of siderosomes
32 would suggest that primary cultured neurons are exhibiting iron “overload” status under typical culture
33 conditions (see methods). If primary cultured neurons were in a state of iron “overload” (hence the
34 formation of siderosomes), one would expect the transferrin receptor to be strongly down regulated.³⁹
35 In contrast, we find that the transferrin receptor is expressed abundantly on the plasma membrane –
36 arguing against the iron “overload” hypothesis (see figs. 3E-G). In addition, ferritin is expressed
37 abundantly (see fig. 3A), so that ferritin storage would be presumed to be normal as well. Thus, our
38 findings would suggest that siderosomes exist in the cytoplasm of primary cultured neurons under
39 typical culture conditions and contain large quantities of iron and some ferritin; with smaller amounts of
40 other metals (but not zinc). Since culture media normally contains significant amounts of iron
41 (Neurobasal culture media contains 250 μ M ferric nitrate), this may be the source of much of this iron,
42 however, it should be noted that iron storage in siderosomes seems not to have an effect on the
43 viability or long term survival of primary neurons maintained in neurobasal media. The lack of toxicity
44 would suggest that this iron is present as insoluble ferric hydroxide (see above). These structures might
45 represent a physiological iron reservoir beyond that provided by ferritin cages. It would be interesting to
46 maintain primary cultured neurons in media with various iron concentrations and compare iron content
47 and distribution by SXRXF with neuron survivability.
48
49
50
51
52
53
54
55
56
57
58
59
60

1
2
3
4
5
6
7
8
9
10
11
12
13
14
15
16
17
18
19
20
21
22
23
24
25
26
27
28
29
30
31
32
33
34
35
36
37
38
39
40
41
42
43
44
45
46
47
48
49
50
51
52
53
54
55
56
57
58
59
60

Insights from zinc loading experiments: Our model for neuronal zinc homeostasis^{11,40} predicted that zinc loads dynamically reside in two pools that we termed “muffler” and “deep store.” Newly acquired zinc is initially bound to the “muffler,” which then shuttles the new zinc to the “deep store.” Whereas, zinc bound to the “muffler” can rapidly move in and out of this pool; zinc can only slowly leave the “deep store.” Thus, the “muffler” is of primary importance in influencing the dynamics of short term or transient changes in cytosolic “free” zinc concentration. The behavior of the two pools is illustrated in fig. 10, which shows zinc levels in the two interacting pools, during transporter mediated zinc uptake. After 3 min, zinc bound to the “muffler” is approaching a steady state, but the zinc is not static. On the contrary, zinc is being shuttled from the “muffler” to the “deep store” and at 3 min, “deep store” zinc is now rapidly rising. The results of SRXRF imaging suggest that both the “muffler” and “deep store” should be considered as diffuse cytosolic buffers, rather than an organelle or single subcellular location or entity inside neurons. The “muffler” and “deep store” are better thought of as being composed of many interacting zinc binding moieties. Does this mean that mitochondria, endoplasmic reticulum and Golgi do not take up and release zinc ions? Certainly it *does not*. However, it can be concluded, based on SRXRF analysis that zinc ions are accumulated in organelle space at a level similar to the average level that exists in the cytoplasm. Organelles expressing membrane bound zinc transporters likely take up and release significant numbers of zinc atoms, but the average total number of atoms in an organelle is similar to that found in a similar sized space in the cytoplasm. It is true however, that nanodomains of high zinc accumulation, if they exist, would likely be masked from detection by SRXRF by the large and uniform distribution of buffered zinc throughout the cytoplasm. In addition, it is fair to presume that since the total concentration of zinc ions is generally uniform in the cytosol and organelles alike, that buffering and hence the “free” concentration is similar as well. If fact, studies using zinc sensors genetically targeted to various organelles bear this out^{12,41} – simply that “free” zinc varies over relatively limited ranges when considering the much larger total zinc quota of the cell.

Our data suggests that zinc transporters have equal density in the cell soma and processes. However, the percentage change in average zinc concentration is much greater in processes than in the soma, since the cellular volume associated with that same surface area is much larger in the soma (and potentially would have greater zinc buffering capacity). This suggests that processes are at greater risk for the deleterious effects of zinc overload due to transporter mediated zinc uptake since transporter density appears to be similar in the processes and the soma. This same principal should be applied to zinc uptake as a result of synaptic activity and mediated by channel proteins.⁴²

Conclusions:

Utilizing synchrotron radiation X-ray fluorescence (SRXRF) to obtain single cell quantitative and subcellular metallomic data, the resting steady state metal quotas for calcium, iron, zinc, copper, manganese, and nickel of primary cortical neurons was determined. Primary cultured neurons typically contain between 100 to 200 million zinc atoms distributed throughout the soma and processes, with an enrichment in the nucleus. When cortical neurons were zinc loaded, the newly acquired zinc was still diffuse and presumably buffered. Soma and processes have about equal abilities to take up zinc. Copper levels are distributed uniformly as well, but are relatively higher in the processes relative to zinc levels.

1
2
3 Iron exhibited a punctate distribution being highly enriched in several puncta in a peri-nuclear location
4 in most neurons, which contained up to 50% of the total neuronal iron content. These puncta are
5 suggested to be iron containing siderosomes existing in the cytoplasm of primary cultured neurons
6 under typical culture conditions and contain large quantities of iron and some ferritin; with smaller
7 amounts of other metals (but not zinc). Iron levels and distribution were determined in primary
8 dopaminergic and non-dopaminergic midbrain neurons. These neurons were similar to cortical neurons
9 in all respects related to their metal content and distribution, including iron levels and the appearance
10 of iron puncta.
11
12
13
14
15

16 **Acknowledgements:** The assistance of Dr. Iain Miller, Department of Biological Sciences, Ohio
17 University, is greatly appreciated for sample preparation and image capture for scanning electron
18 microscopy. This research used resources of the Advanced Photon Source, a U.S. Department of Energy
19 (DOE) Office of Science User Facility operated for the DOE Office of Science by Argonne National
20 Laboratory under Contract No. DE-AC02-06CH11357. This work was partially supported and Ohio
21 University Research Committee (OURC) and Baker Fund Awards, Ohio University (to RAC & DL), by the
22 Ohio Musculoskeletal and Neurological Institute (OMNI) and the Flagship Grant from Korea Institute of
23 Science and Technology (Brain Science Institute), Seoul, Korea (to DL).
24
25
26
27
28
29

30 **Figure legends:**

31
32 **Figure 1:** Representative 2-D scans derived from SRXRF data and line scan data of a cryofixed and
33 dehydrated primary cortical neuron. The relative intensity rainbow scale used is shown below the zinc
34 scan (A) – red is highest, black is lowest – ng/cm². Size calibration is shown as a black bar, lower right
35 corner of the zinc scan = 2 micron. (A) zinc, (B) phosphorous, (C) sulfur, (D) calcium, (E) iron, (F) copper,
36 (G) manganese. Just to the left of the SRXRF line scans is the zinc 2-D scan shown in A; the red arrow
37 shows the location and direction of the line scan that produced the plots: (H) zinc and sulfur; (I) zinc and
38 phosphorous; (J) zinc and iron; (K) zinc and calcium; (L) iron and calcium.
39
40
41
42

43 **Figure 2:** Plots comparing the average metal contents in regions of interest (ROI) manually drawn using
44 MAPS software around iron puncta (identified in 2-D SRXRF scans; see fig. 1C for an example) or the
45 entire neuronal soma (see fig. 1D for an example). Metal contents are expressed for each ROI as the
46 average value – ng/cm². Data presented are the mean ± S.E., n = at least 9 single neurons, at most n = 11
47 single neurons; two separate trips to APS beamline. Comparing pairs of means for each metal (i.e., soma
48 vs. iron puncta), Student's t-test was significant ($p < 0.05$) for Zn, Mn, Ni, and Cu and $p < 0.0001$ for Fe;
49 no significant difference in the means for Ca. (A) calcium, iron, and zinc, (B) manganese, nickel, and
50 copper.
51
52
53
54
55

56 **Figure 3:** Representative immunofluorescence images from primary cortical neurons showing the
57 subcellular localization and relative expression level of ferritin light chain, transferrin receptor, and
58
59
60

1
2
3
4
5
6
7
8
9
10
11
12
13
14
15
16
17
18
19
20
21
22
23
24
25
26
27
28
29
30
31
32
33
34
35
36
37
38
39
40
41
42
43
44
45
46
47
48
49
50
51
52
53
54
55
56
57
58
59
60

LC3B; proteins important in neuronal iron homeostasis. **(A)** Image shows ferritin light chain immunofluorescence; nucleus made fluorescent with DAPI. Arrows point to apparent larger aggregates of ferritin light chain. **(B)** Image shows immunofluorescence for ferritin light chain, **(C)** immunofluorescence for LC3B, and **(D)** an overlay of images **B** and **C**; nucleus made fluorescent with DAPI. **(E)** Image shows immunofluorescence for transferrin receptor; arrows point to neuronal processes expressing transferrin receptor; nucleus made fluorescent with DAPI. Note lack of immunofluorescence in the soma. **(F)** Image of the same neuron, but at a different plane of focus, showing the soma and apparent transferrin receptor expression at the plasma membrane; nucleus made fluorescent with DAPI. **(G)** Image of immunofluorescence for transferrin receptor associated with the nuclear membrane; arrows point to regions of exceptionally bright transferrin receptor immunofluorescence; nucleus made fluorescent with DAPI. Scale bar on all images = 10 micron

Figure 4: Quantitative metallomics of cryofixed and dehydrated neuronal processes from SRXRF 2-D scans of single primary cortical neurons. Regions of interest (ROI) were manually drawn around neuronal processes randomly selected in 2-D SRXRF scans using MAPS software. Metal levels are expressed for each ROI as the average value – ng/cm². Data presented are the mean ± S.E., n = 4 (Ca, Cu), n = 5 (Fe, Zn), cryofixed and dehydrated neuronal processes, one trip to APS beamline.

Figure 5: Quantitative and spatial metallomics of cryofixed single primary cortical neurons before and after a 30 min (37°C) exposure to 30 μM ZnCl₂ and 5 μM pyrithione. Regions of interest (ROI) were manually drawn around neuronal soma observed in 2-D SRXRF scans using MAPS software. Metal levels are expressed as total atoms per each ROI. Note that the y-axis is a log scale. Scatter plots (horizontal bar represents the mean of all measurements for that experimental condition); **(A)** iron, copper, and zinc; and **(B)** Manganese and nickel. **(C)** Line scan of two similarly sized and shaped cryofixed and dehydrated primary cortical neurons overlaid on the same plot. One neuron is control resting conditions, the second neuron was exposed to zinc and pyrithione as described above. The horizontal line helps to illustrate the “flattening” of the zinc profile after zinc and pyrithione treatment. Comparing pairs of means for each metal (i.e., control vs. ZnCl₂ and pyrithione – ZP30), Student’s t-test was significant ($p < 0.0001$) for Fe, Zn, and Ni, $p < 0.05$ for Ca and Mn, and not significant for Fe.

Figure 6: Zinc levels in neuronal soma and iron puncta from SRXRF 2-D scans of cryofixed and dehydrated single primary cortical neurons with (ZP30) or without (control) a 30 min (37°C) exposure to 30 μM ZnCl₂ and 5 μM pyrithione. Regions of interest (ROI) were manually drawn around neuronal soma and iron puncta observed in 2-D SRXRF scans using MAPS software. Zinc levels are expressed for each ROI as the average value – ng/cm². Data presented are the mean ± S.E., numbers in parentheses equals the number of single soma or iron puncta analyzed. Student’s t-test was significant ($p < 0.05$) for average zinc level in control soma vs. control iron puncta.

Figure 7: Quantitative and spatial metallomics of cryofixed single primary cortical neurons before and after a 3 min (37°C) exposure to 30 μM ZnCl₂. Regions of interest (ROI) were manually drawn around neuronal soma observed in 2-D SRXRF scans using MAPS software. Metal levels are expressed as total atoms per each ROI. Note that the y-axis is a log scale. Scatter plots (horizontal bar represents the mean

1
2
3 of all measurements for that experimental condition); **(A)** iron, copper, and zinc; and **(B)** Manganese and
4 nickel. **(C)** Line scan of two similarly sized and shaped cryofixed and dehydrated primary cortical neurons
5 overlaid on the same plot. One neuron is control resting conditions, the second neuron was exposed
6 to zinc as described above. The arrows point to cytoplasmic regions of the neurons where the most zinc
7 appears to accumulate. Comparing pairs of means for each metal (i.e., control vs. ZnCl₂ 3 min – Zn3M),
8 Student's t-test was significant ($p < 0.0001$) for Zn only.
9
10

11
12
13
14 **Figure 8:** Quantitative metallomics of cryofixed neuronal processes from SRXRF 2-D scans of single
15 primary cortical neurons before and after a 3 min (37°C) exposure to 30 μM ZnCl₂. Regions of interest
16 (ROI) were manually drawn around neuronal processes randomly selected in 2-D SRXRF scans using
17 MAPS software. Metal levels are expressed for each ROI as the average value – ng/cm². Data presented
18 are the mean ± S.E., numbers in parentheses equals the number of single processes or somas analyzed.
19 Comparing pairs of means for each condition (i.e., control processes vs. ZnCl₂ 3 min processes or control
20 soma vs. ZnCl₂ 3 min soma), Student's t-test was significant ($p < 0.0001$) for processes; $p = 0.1538$ for
21 soma.
22
23
24
25

26 **Figure 9:** Quantitative metallomics of chemically fixed and dehydrated single primary dopaminergic,
27 non-dopaminergic, and hippocampal neurons derived from SRXRF 2-D scans. **(A)** Dopaminergic neurons
28 were identified as tyrosine hydroxylase positive by immunofluorescence; nucleus made fluorescent with
29 DAPI. Note the fluorescent neurons (DOPA) that are neighboring non-fluorescent neurons (but which
30 can be seen because of nuclear DAPI fluorescence); the tyrosine hydroxylase negative neurons on the
31 same SiN windows were labeled as non-dopaminergic. Scale bar = 20 micron. **(B)** Metal levels for copper
32 and zinc; **(C)** metal levels for manganese and nickel; **(D)** iron levels in iron puncta and in the soma.
33 Regions of interest (ROI) were manually drawn around neuronal soma and iron puncta observed in 2-D
34 SRXRF scans using MAPS software. Metal levels are expressed for each ROI as an average value –
35 ng/cm². Data presented are the mean ± S.E., no significant differences were found when comparing the
36 means ($p > 0.05$); one way analysis of variance with Tukey's multiple comparisons posttest. The number
37 in parentheses equals the number of iron puncta or single neuronal soma analyzed for metal content.
38 Note that the number of soma analyzed applies to figs. B-D.
39
40
41
42
43

44 **Figure 10:** Model predictions for changes in zinc concentration in the “muffler” and “deep store” pools
45 during transporter mediated zinc uptake. See text for additional explanation. Model development and
46 detailed explanations are published.¹¹
47
48
49
50
51
52
53
54
55
56
57
58
59
60

Table I.

Table I. Comparison of Zinc and Copper Content in Neuronal Processes and Cell Somas as Determined by SRXRF 2-D Scans, Control and After Transporter Mediated Zinc Loading		
Experimental condition	Zinc (ng/cm²) mean ± S.E. (n)	Copper (ng/cm²) mean ± S.E. (n)
Control Processes	3.97 ± 0.39 (5)	0.40 ± 0.14 (5)
Control Somas	17.9 ± 3.00 (6)	0.81 ± 0.11 (6)
Zinc Loaded Processes	9.62 ± 0.67 (9)	0.21 ± 0.04 (9)
Zinc Loaded Somas	24.3 ± 2.71 (5)	0.55 ± 0.05 (5)

n = the number of ROIs analyzed, neurons were loaded with zinc by incubation with 30 μM ZnCl₂ for 3 min.

Table II.

Table II. Total Metal Quotas in Single Cortical Neurons as Determined by SRXRF 2-D Scans		
Metal (number of neurons scanned)	Method of Sample Preparation	Millions of Atoms (mean)
Calcium (9)	Chemical fixation	2,360
Zinc (15)	Cryofixation	163
Iron (15)	Cryofixation	119
Copper (15)	Cryofixation	7.86
Manganese (15)	Cryofixation	11.8
Nickel (14)	Cryofixation	2.62

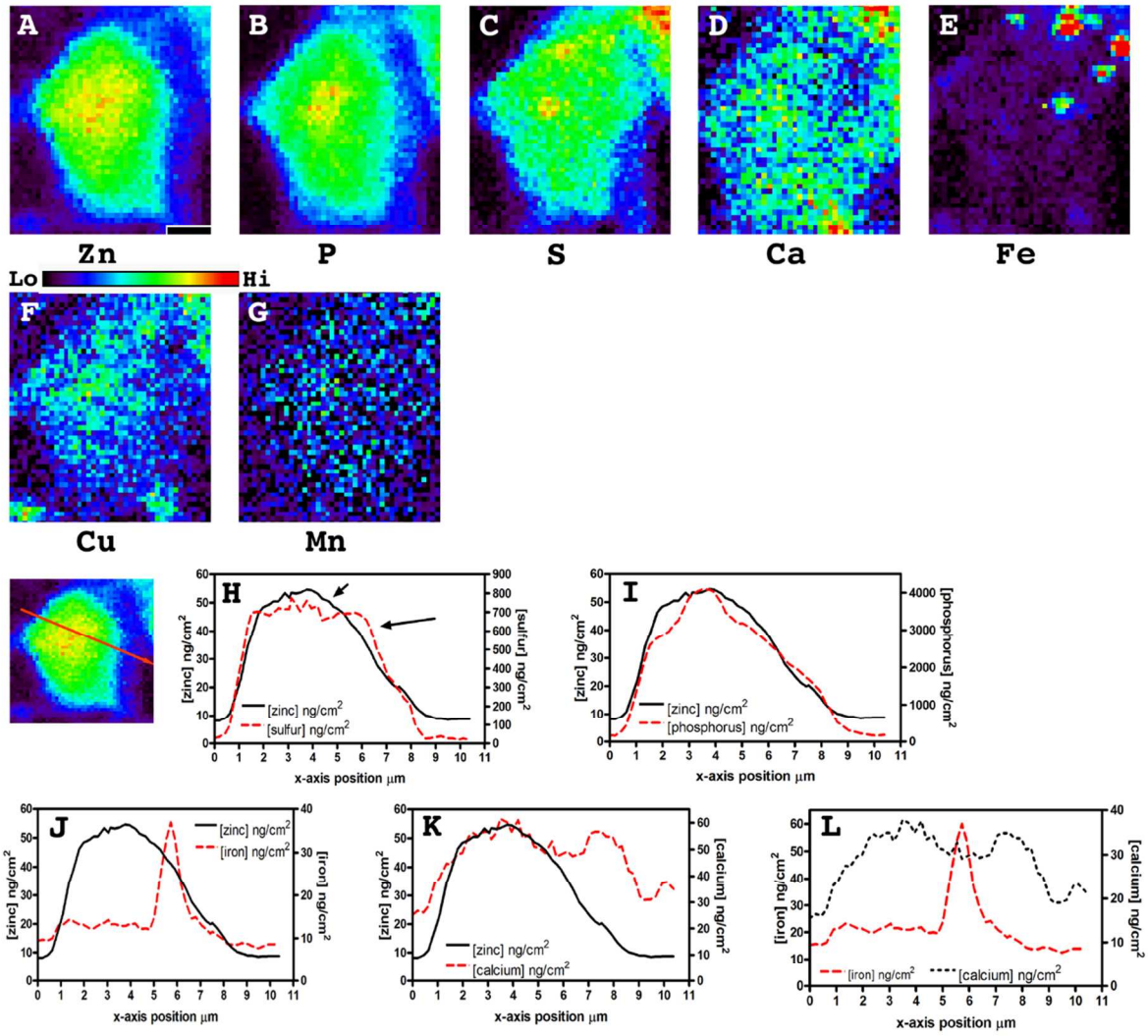
References:

1. C. J. Fahrni, Biological applications of X-ray fluorescence microscopy: exploring the subcellular topography and speciation of transition metals. *Curr Opin Chem Biol* 2007, *11*. 121-7, DOI: 10.1016/j.cbpa.2007.02.039.
2. R. Ortega, G. Deves, A. Carmona, Bio-metals imaging and speciation in cells using proton and synchrotron radiation X-ray microspectroscopy. *J R Soc Interface* 2009, *6 Suppl 5*. S649-58, DOI: 10.1098/rsif.2009.0166.focus.
3. G. D. Ciccotosto, S. A. James, M. Altissimo, D. Paterson, S. Vogt, B. Lai, M. D. de Jonge, D. L. Howard, A. I. Bush, R. Cappai, Quantitation and localization of intracellular redox active metals by X-ray fluorescence microscopy in cortical neurons derived from APP and APLP2 knockout tissue. *Metallomics* 2014, *6*. 1894-1904, DOI: 10.1039/c4mt00176a.
4. T. Dučić, E. Barski, M. Salome, J. C. Koch, M. Bähr, P. Lingor, X-ray fluorescence analysis of iron and manganese distribution in primary dopaminergic neurons. *Journal of Neurochemistry* 2013, *124*. 250-261, DOI: 10.1111/jnc.12073.
5. R. A. Colvin, C. J. Stork, Y. V. Li, B. Lai, in *Metal Ion in Stroke*, ed. Y. V. Li, J. H. Zhang. Springer: New York, 2012, pp 227-237.
6. S. W. Suh, J. W. Chen, M. Motamedi, B. Bell, K. Listiak, N. F. Pons, G. Danscher, C. J. Frederickson, Evidence that synaptically-released zinc contributes to neuronal injury after traumatic brain injury. *Brain Res* 2000, *852*. 268-73.
7. A. I. Bush, C. C. Curtain, Twenty years of metallo-neurobiology: where to now? *Eur Biophys J* 2008, *37*. 241-5.
8. S. L. Sensi, P. Paoletti, A. I. Bush, I. Sekler, Zinc in the physiology and pathology of the CNS. *Nat Rev Neurosci* 2009, *10*. 780-91, DOI: 10.1038/nrn2734.
9. T. A. Rouault, Iron metabolism in the CNS: implications for neurodegenerative diseases. *Nat Rev Neurosci* 2013, *14*. 551-564, DOI: 10.1038/nrn3453.
10. L. Zecca, M. B. Youdim, P. Riederer, J. R. Connor, R. R. Crichton, Iron, brain ageing and neurodegenerative disorders. *Nat Rev Neurosci* 2004, *5*. 863-73, DOI: 10.1038/nrn1537.
11. R. A. Colvin, A. I. Bush, I. Volitakis, C. P. Fontaine, D. Thomas, K. Kikuchi, W. R. Holmes, Insights into Zn²⁺ homeostasis in neurons from experimental and modeling studies. *Am J Physiol Cell Physiol* 2008, *294*. C726-42, DOI: 10.1152/ajpcell.00541.2007.
12. P. Chabosseau, E. Tuncay, G. Meur, E. A. Bellomo, A. Hessels, S. Hughes, P. R. V. Johnson, M. Bugliani, P. Marchetti, B. Turan, A. R. Lyon, M. Merx, G. A. Rutter, Mitochondrial and ER-Targeted eCALWY Probes Reveal High Levels of Free Zn²⁺. *ACS Chemical Biology* 2014, *9*. 2111-2120, DOI: 10.1021/cb5004064.
13. Y. Qin, P. J. Dittmer, J. G. Park, K. B. Jansen, A. E. Palmer, Measuring steady-state and dynamic endoplasmic reticulum and Golgi Zn²⁺ with genetically encoded sensors. *Proc Natl Acad Sci U S A* 2011, *108*. 7351-6, DOI: 10.1073/pnas.1015686108.
14. R. Ortega, P. Cloetens, G. Deves, A. Carmona, S. Bohic, Iron storage within dopamine neurovesicles revealed by chemical nano-imaging. *PLoS ONE* 2007, *2*. e925, DOI: 10.1371/journal.pone.0000925.
15. A. Carmona, P. Cloetens, G. Deves, S. Bohic, R. Ortega, Nano-imaging of trace metals by synchrotron X-ray fluorescence into dopaminergic single cells and neurite-like processes. *Journal of Analytical Atomic Spectrometry* 2008, *23*. 1083-1088, DOI: 10.1039/b802242a.

- 1
2
3
4
5
6
7
8
9
10
11
12
13
14
15
16
17
18
19
20
21
22
23
24
25
26
27
28
29
30
31
32
33
34
35
36
37
38
39
40
41
42
43
44
45
46
47
48
49
50
51
52
53
54
55
56
57
58
59
60
16. R. A. Colvin, M. Laskowski, C. P. Fontaine, Zinquin identifies subcellular compartmentalization of zinc in cortical neurons. Relation to the trafficking of zinc and the mitochondrial compartment. *Brain Res* 2006, *1085*. 1-10, DOI: 10.1016/j.brainres.2006.02.043.
 17. R. A. Colvin, pH dependence and compartmentalization of zinc transported across plasma membrane of rat cortical neurons. *Am J Physiol Cell Physiol* 2002, *282*. C317-29, DOI: 10.1152/ajpcell.00143.2001.
 18. T. Fath, Y. D. Ke, P. Gunning, J. Gotz, L. M. Ittner, Primary support cultures of hippocampal and substantia nigra neurons. *Nat Protoc* 2009, *4*. 78-85, DOI: 10.1038/nprot.2008.199.
 19. R. McRae, B. Lai, S. Vogt, C. J. Fahrni, Correlative microXRF and optical immunofluorescence microscopy of adherent cells labeled with ultrasmall gold particles. *J Struct Biol* 2006, *155*. 22-9.
 20. Z. Qin, B. Toursarkissian, B. Lai, Synchrotron radiation X-ray fluorescence microscopy reveals a spatial association of copper on elastic laminae in rat aortic media. *Metalloomics* 2011, *3*. 823-828.
 21. S. Vogt, MAPS: A set of software tools for analysis and visualization of 3D X-ray fluorescence data sets. *Journal of Physiology IV* 2003, *104*. 635-638.
 22. L. Wiemerslage, B. J. Schultz, A. Ganguly, D. Lee, Selective degeneration of dopaminergic neurons by MPP(+) and its rescue by D2 autoreceptors in Drosophila primary culture. *J Neurochem* 2013, *126*. 529-40, DOI: 10.1111/jnc.12228.
 23. S. A. James, M. D. de Jonge, D. L. Howard, A. I. Bush, D. Paterson, G. McColl, Direct in vivo imaging of essential bioinorganics in Caenorhabditis elegans. *Metalloomics* 2013, *5*. 627-635, DOI: 10.1039/c3mt00010a.
 24. D. J. Hare, J. L. George, L. Bray, I. Volitakis, A. Vais, T. M. Ryan, R. A. Cherny, A. I. Bush, C. L. Masters, P. A. Adlard, P. A. Doble, D. I. Finkelstein, The effect of paraformaldehyde fixation and sucrose cryoprotection on metal concentration in murine neurological tissue. *Journal of Analytical Atomic Spectrometry* 2014, *29*. 565-570, DOI: 10.1039/c3ja50281c.
 25. M. J. Hackett, J. A. McQuillan, F. El-Assaad, J. B. Aitken, A. Levina, D. D. Cohen, R. Siegele, E. A. Carter, G. E. Grau, N. H. Hunt, P. A. Lay, Chemical alterations to murine brain tissue induced by formalin fixation: implications for biospectroscopic imaging and mapping studies of disease pathogenesis. *Analyst* 2011, *136*. 2941-52, DOI: 10.1039/c0an00269k.
 26. M. Schrag, A. Dickson, A. Jiffry, D. Kirsch, H. Vinters, W. Kirsch, The effect of formalin fixation on the levels of brain transition metals in archived samples. *BioMetals* 2010, *23*. 1123-1127, DOI: 10.1007/s10534-010-9359-4.
 27. D. C. Johnson, D. R. Dean, A. D. Smith, M. K. Johnson, Structure, function, and formation of biological iron-sulfur clusters. *Annu Rev Biochem* 2005, *74*. 247-81, DOI: 10.1146/annurev.biochem.74.082803.133518.
 28. T. A. Rouault, Mammalian iron-sulphur proteins: novel insights into biogenesis and function. *Nat Rev Mol Cell Biol* 2015, *16*. 45-55, DOI: 10.1038/nrm3909.
 29. T. Asano, M. Komatsu, Y. Yamaguchi-Iwai, F. Ishikawa, N. Mizushima, K. Iwai, Distinct mechanisms of ferritin delivery to lysosomes in iron-depleted and iron-replete cells. *Mol Cell Biol* 2011, *31*. 2040-52, DOI: 10.1128/MCB.01437-10.
 30. J. D. Mancias, X. Wang, S. P. Gygi, J. W. Harper, A. C. Kimmelman, Quantitative proteomics identifies NCOA4 as the cargo receptor mediating ferritinophagy. *Nature* 2014. DOI: 10.1038/nature13148.
 31. E. D. Gaier, B. A. Eipper, R. E. Mains, Copper signaling in the mammalian nervous system: Synaptic effects. *Journal of Neuroscience Research* 2013, *91*. 2-19, DOI: 10.1002/jnr.23143.
 32. A. Krezel, W. Maret, Zinc-buffering capacity of a eukaryotic cell at physiological pZn. *J Biol Inorg Chem* 2006, *11*. 1049-62.

- 1
2
3
4
5
6
7
8
9
10
11
12
13
14
15
16
17
18
19
20
21
22
23
24
25
26
27
28
29
30
31
32
33
34
35
36
37
38
39
40
41
42
43
44
45
46
47
48
49
50
51
52
53
54
55
56
57
58
59
60
33. E. Kosior, S. Bohic, H. Suhonen, R. Ortega, G. Deves, A. Carmona, F. Marchi, J. F. Guillet, P. Cloetens, Combined use of hard X-ray phase contrast imaging and X-ray fluorescence microscopy for sub-cellular metal quantification. *J Struct Biol* 2012, *177*. 239-47, DOI: 10.1016/j.jsb.2011.12.005.
34. W. Maret, Zinc biochemistry: from a single zinc enzyme to a key element of life. *Advances in nutrition* 2013, *4*. 82-91, DOI: 10.3945/an.112.003038.
35. A. W. Foster, D. Osman, N. J. Robinson, Metal Preferences and Metallation. *Journal of Biological Chemistry* 2014, *289*. 28095-28103, DOI: 10.1074/jbc.R114.588145.
36. I. Irving, R. J. P. Williams, Order of stability of metal complexes. *Nature (London)* 1948, *162*. 746-747.
37. F. N. Ghadially, in *Ultrastructural Pathology of the Cell and Matrix*, ed. F. N. Ghadially. Butterworth-Heinemann: Boston, 4th edn., 1997, vol. 2, pp 668-674.
38. S. Sato, G. F. Murphy, J. D. Bernhard, M. C. Mihm, Jr., T. B. Fitzpatrick, Ultrastructural and x-ray microanalytical observations of minocycline-related hyperpigmentation of the skin. *The Journal of investigative dermatology* 1981, *77*. 264-71.
39. B. X. Wong, J. A. Duce, The iron regulatory capability of the major protein participants in prevalent neurodegenerative disorders. *Frontiers in pharmacology* 2014, *5*. 81, DOI: 10.3389/fphar.2014.00081.
40. R. A. Colvin, W. R. Holmes, C. P. Fontaine, W. Maret, Cytosolic zinc buffering and muffling: their role in intracellular zinc homeostasis. *Metallomics* 2010, *2*. 306-17, DOI: 10.1039/b926662c.
41. P. J. Dittmer, J. G. Miranda, J. A. Gorski, A. E. Palmer, Genetically encoded sensors to elucidate spatial distribution of cellular zinc. *J Biol Chem* 2009, *284*. 16289-97, DOI: 10.1074/jbc.M900501200.
42. R. A. Colvin, C. P. Fontaine, M. Laskowski, D. Thomas, Zn²⁺ transporters and Zn²⁺ homeostasis in neurons. *Eur J Pharmacol* 2003, *479*. 171-85.

Figure 1:



1
2
3
4
5
6
7
8
9
10
11
12
13
14
15
16
17
18
19
20
21
22
23
24
25
26
27
28
29
30
31
32
33
34
35
36
37
38
39
40
41
42
43
44
45
46
47
48
49
50
51
52
53
54
55
56
57
58
59
60

Figure 2:

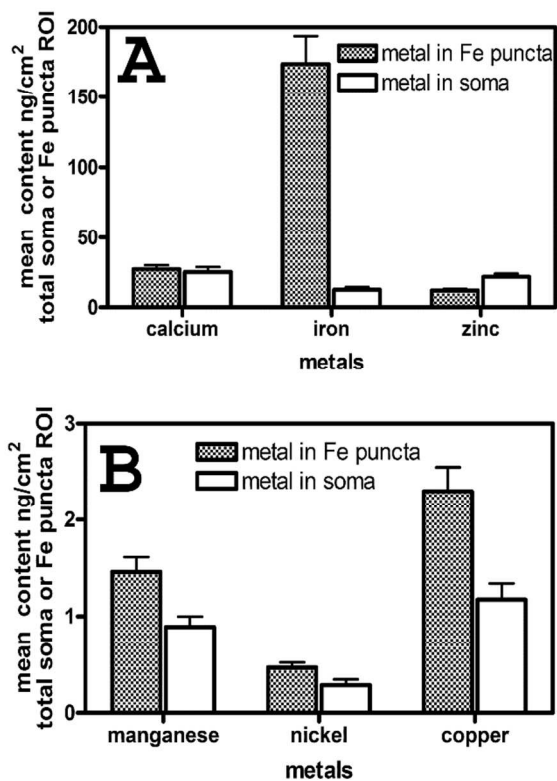
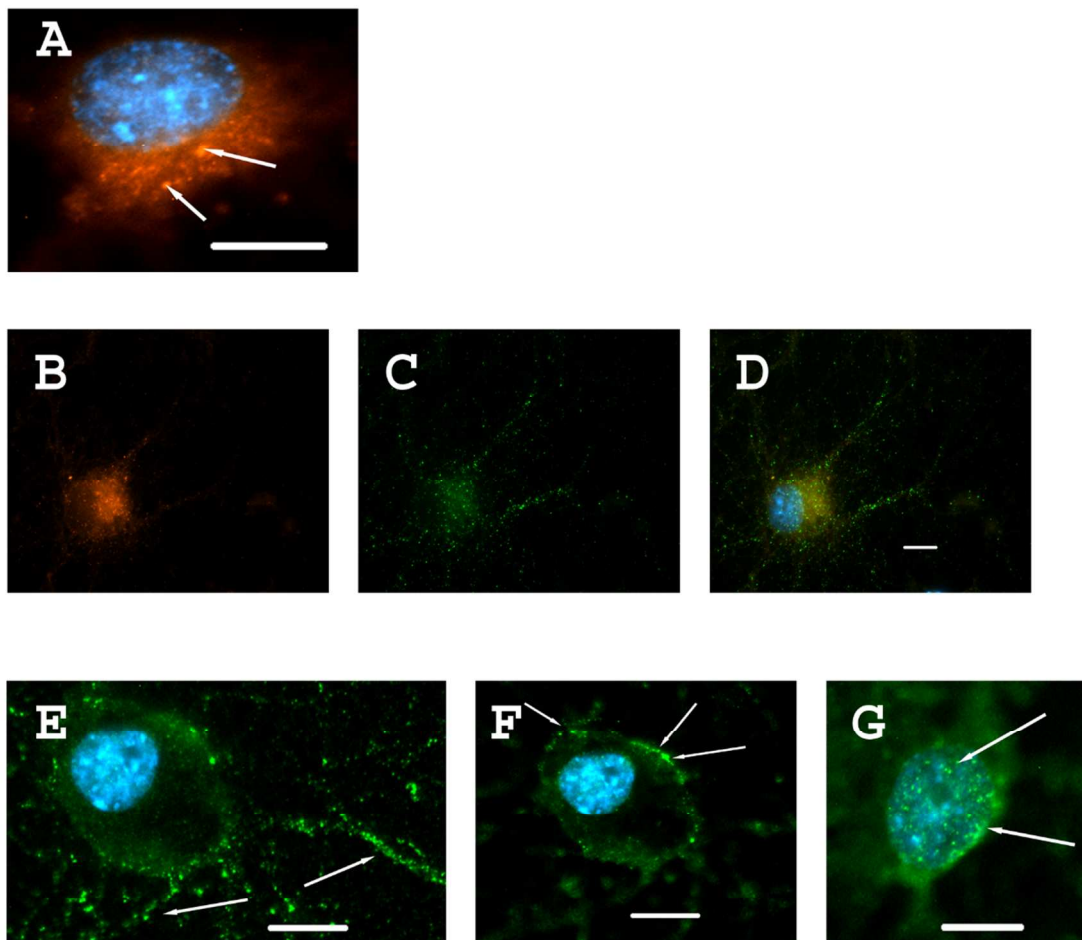
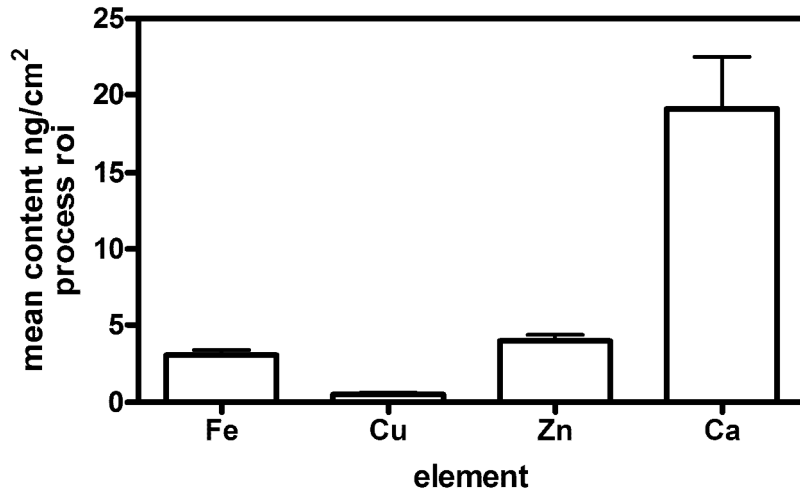


Figure 3:



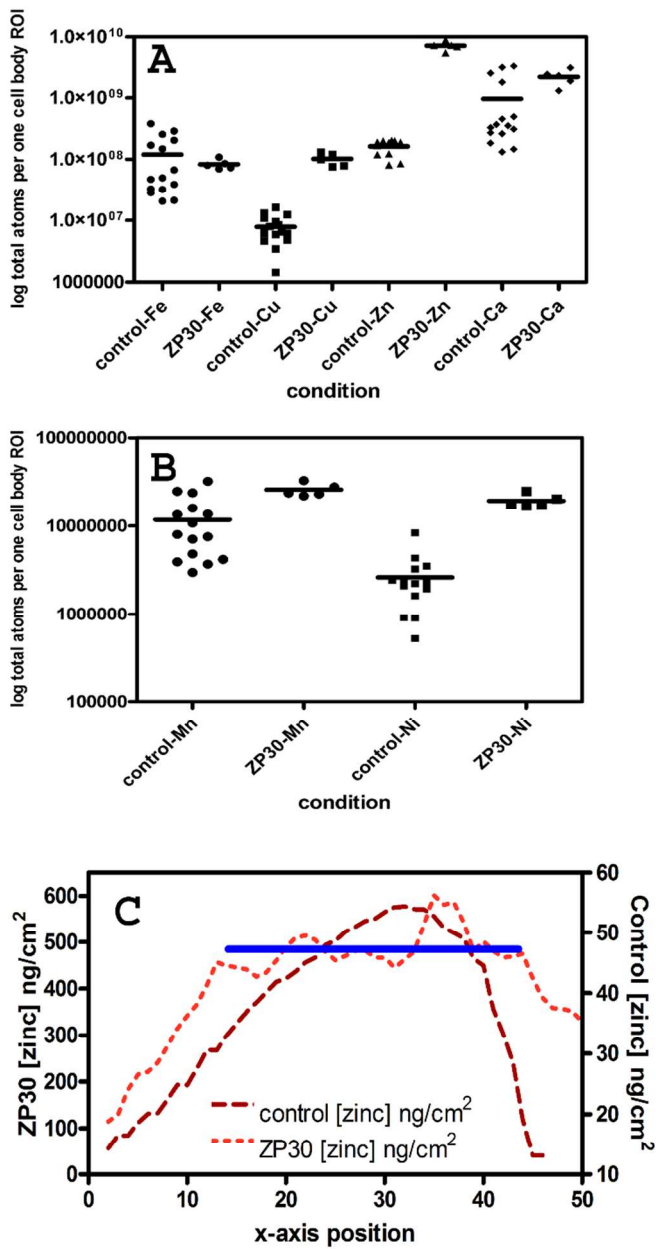
1
2
3
4
5
6
7
8
9
10
11
12
13
14
15
16
17
18
19
20
21
22
23
24
25
26
27
28
29
30
31
32
33
34
35
36
37
38
39
40
41
42
43
44
45
46
47
48
49
50
51
52
53
54
55
56
57
58
59
60

Figure 4:



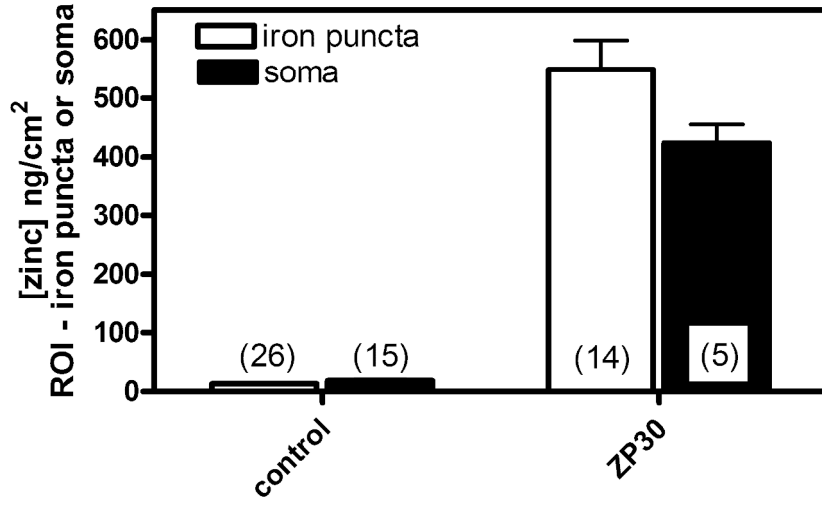
1
2
3
4
5
6
7
8
9
10
11
12
13
14
15
16
17
18
19
20
21
22
23
24
25
26
27
28
29
30
31
32
33
34
35
36
37
38
39
40
41
42
43
44
45
46
47
48
49
50
51
52
53
54
55
56
57
58
59
60

Figure 5:



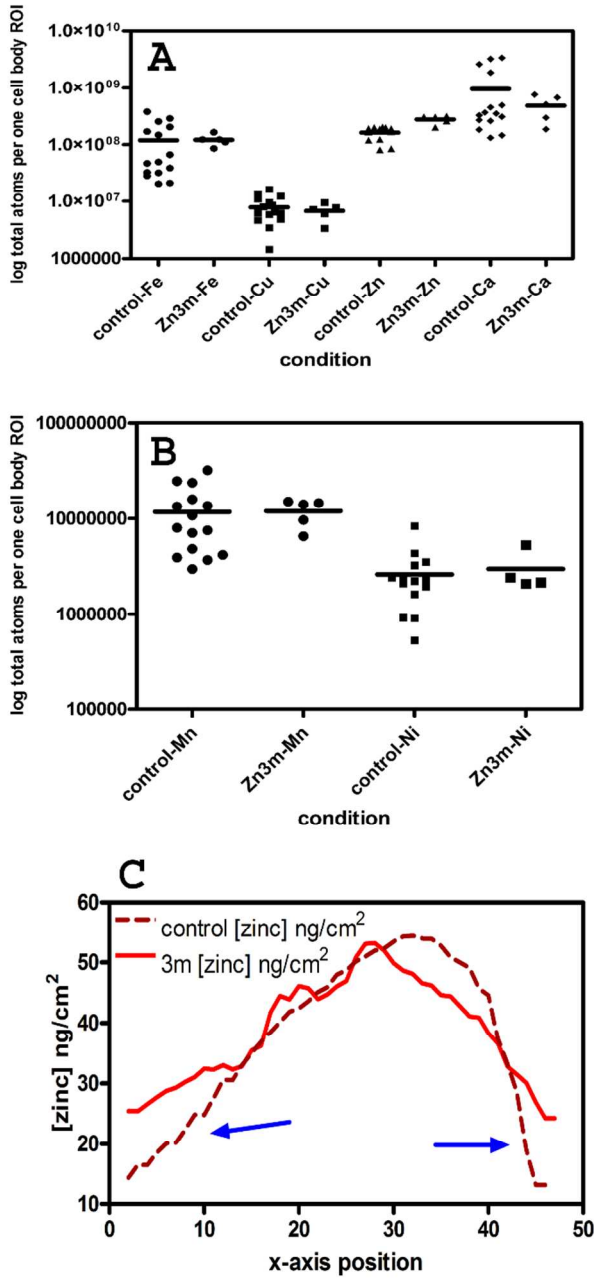
1
2
3
4
5
6
7
8
9
10
11
12
13
14
15
16
17
18
19
20
21
22
23
24
25
26
27
28
29
30
31
32
33
34
35
36
37
38
39
40
41
42
43
44
45
46
47
48
49
50
51
52
53
54
55
56
57
58
59
60

Figure 6:



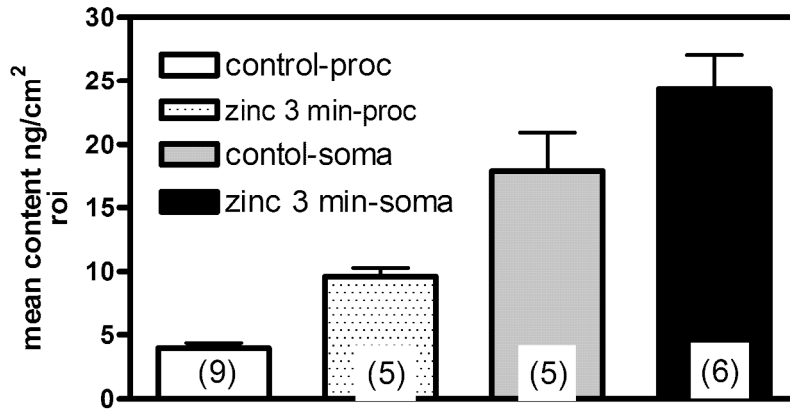
1
2
3
4
5
6
7
8
9
10
11
12
13
14
15
16
17
18
19
20
21
22
23
24
25
26
27
28
29
30
31
32
33
34
35
36
37
38
39
40
41
42
43
44
45
46
47
48
49
50
51
52
53
54
55
56
57
58
59
60

Figure 7:



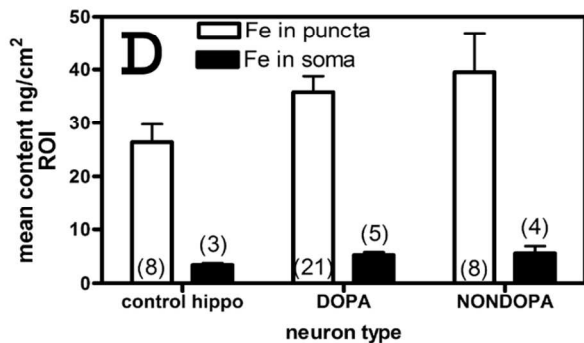
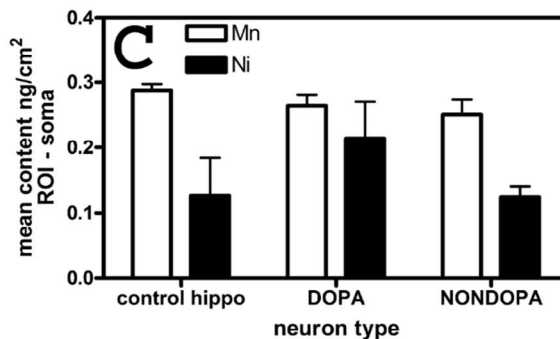
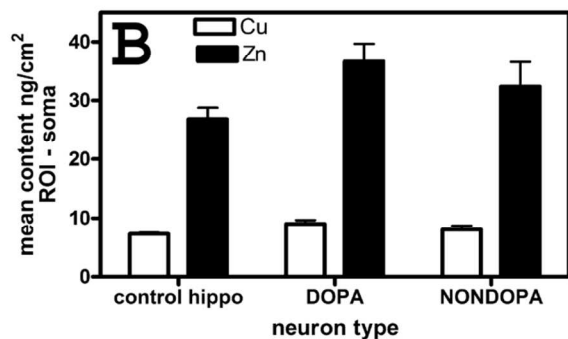
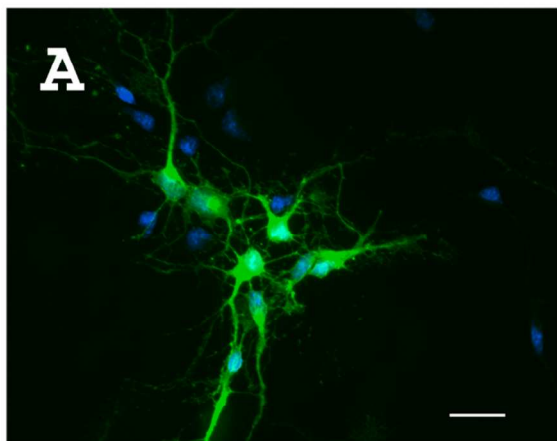
1
2
3
4
5
6
7
8
9
10
11
12
13
14
15
16
17
18
19
20
21
22
23
24
25
26
27
28
29
30
31
32
33
34
35
36
37
38
39
40
41
42
43
44
45
46
47
48
49
50
51
52
53
54
55
56
57
58
59
60

Figure 8:



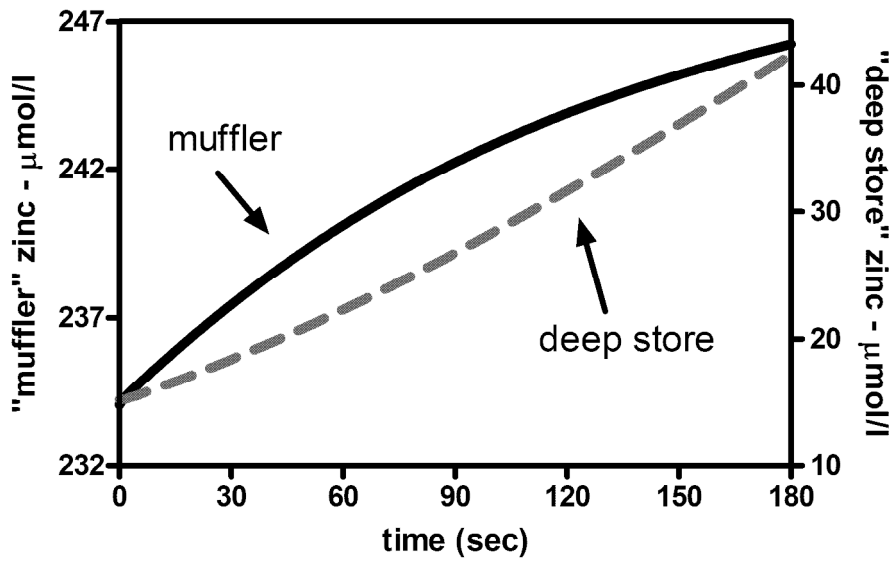
1
2
3
4
5
6
7
8
9
10
11
12
13
14
15
16
17
18
19
20
21
22
23
24
25
26
27
28
29
30
31
32
33
34
35
36
37
38
39
40
41
42
43
44
45
46
47
48
49
50
51
52
53
54
55
56
57
58
59
60

Figure 9:



1
2
3
4
5
6
7
8
9
10
11
12
13
14
15
16
17
18
19
20
21
22
23
24
25
26
27
28
29
30
31
32
33
34
35
36
37
38
39
40
41
42
43
44
45
46
47
48
49
50
51
52
53
54
55
56
57
58
59
60

Figure 10:



1
2
3
4
5
6
7
8
9
10
11
12
13
14
15
16
17
18
19
20
21
22
23
24
25
26
27
28
29
30
31
32
33
34
35
36
37
38
39
40
41
42
43
44
45
46
47
48
49
50
51
52
53
54
55
56
57
58
59
60